JGR Atmospheres

RESEARCH ARTICLE
10.1029/2021JD036376

Megadrought: A Series of Unfortunate La Niña Events?

Carlos M. Carrillo[1], Sloan Coats[2], Matt Newman[3,4], Dimitris A. Herrera[1], Xiaolu Li[1], Rick Moore[1], Sang-Ik Shin[3], Samantha Stevenson[5], Flavio Lehner[1,6], and Toby R. Ault[1]

[1]Earth and Atmospheric Sciences, Cornell University, NY, Ithaca, USA, [2]Department of Earth Sciences, University of Hawaii, HI, Manoa, USA, [3]CIRES Climate Diagnostic Center, University of Colorado, Boulder, CO, USA, [4]Physical Sciences Division, NOAA/Earth System Research Laboratory, Boulder, CO, USA, [5]Bren School of Environmental Science & Management, University of California-Santa Barbara, Santa Barbara, CA, USA, [6]Climate and Global Dynamics Laboratory, National Center for Atmospheric Research, Boulder, CO, USA

Key Points:

- Low-frequency variability in the tropical Pacific is not critical for producing megadroughts in the US Southwest
- A hybrid modeling approach confirms the statistically significant occurrence of megadrought in the SWUS similar to paleoclimate records
- A statistically plausible series of La Niña events may be sufficient to generate megadrought

Supporting Information:

Supporting Information may be found in the online version of this article.

Correspondence to:

C. M. Carrillo,
carrillo@cornell.edu

Citation:

Carrillo, C. M., Coats, S., Newman, M., Herrera, D. A., Li, X., Moore, R., et al. (2022). Megadrought: A series of unfortunate La Niña events? *Journal of Geophysical Research: Atmospheres*, *127*, e2021JD036376. https://doi.org/10.1029/2021JD036376

Received 19 DEC 2021
Accepted 21 SEP 2022

Abstract Megadroughts are multidecadal periods of aridity more persistent than most droughts during the instrumental period. Paleoclimate evidence suggests that megadroughts occur in many parts of the world, including North America, Central America, western Europe, eastern Asia, and northern Africa. It remains unclear to what extent such megadroughts require external forcing or whether they can arise from internal climate variability alone. A novel statistical–dynamical approach is used to evaluate the possibility that such events arise solely as a function of interannual tropical sea surface temperature (SST) variations. A statistical emulator of tropical SST variations is constructed by using an empirical moving-blocks bootstrap approach that randomly samples multiyear sequences of the observational SST record. This approach preserves the power spectrum, seasonal cycle, and spatial pattern of El Niño-Southern Oscillation (ENSO) but removes longer timescale fluctuations embedded in the observational record. These resampled SST anomalies are then used to force an atmospheric model (the Community Atmosphere Model Version 5). As megadroughts emerge in this run, they should, therefore, be solely a consequence of La Niña sequences combined with internal atmospheric variability and persistence driven by soil moisture storage and other land-surface processes. We indeed find that megadroughts in this simulation have an amplitude-duration rate that is generally indistinguishable from the rate documented in paleoclimate records of the western United States. Our findings support the idea that megadroughts may occur randomly when the unforced climate system evolves freely over a sufficiently long period of time, implying that an unforced unusual but statistically plausible series of La Niña events may be sufficient to generate megadrought.

1. Introduction

Megadroughts are multidecadal periods of aridity as severe as the 1930s "Dust Bowl," but much longer lasting (Ault & George, 2018; Ault et al., 2014; B. I. Cook et al., 2016; Woodhouse & Overpeck, 1998). During the past millennium, paleoclimate records indicate that megadroughts occurred throughout the western US, northern Mexico, and many other parts of the world (B. I. Cook et al., 2016). Their long duration may have imposed unprecedented water stresses on several preindustrial civilizations, contributing to their collapse (e.g., Benson et al., 2007; B. I. Cook et al., 2016). Furthermore, the odds that they will occur during this millennium are increasing due to rising regional temperatures and changing global circulation patterns (Ault et al., 2014, 2016; B. I. Cook et al., 2015). Despite the importance of characterizing the hazards imposed on water resources by megadroughts, it remains unclear whether such prolonged climate events in the past emerged in response to exogenous radiative forcing (e.g., solar irradiance, volcanic eruptions, or orbital trends), as a consequence of internal climate variability on multidecadal to centennial timescales (e.g., Ault et al., 2018; Coats, Smerdon, Seager, et al., 2013; Stevenson et al., 2015), or as a function of unusual, but unforced, drought episodes on interannual timescales that collectively produce a megadrought (Ault et al., 2018; Coats et al., 2015). Here, we explore this possibility by asking if an unusual, but inherently random series of La Niña events would be able to produce megadroughts.

Because megadroughts are infrequent events that have only occurred once or twice per millennium, two basic approaches have been employed to understand their nature using both dynamical and statistical models (e.g., Ault et al., 2018; Coats et al., 2015; B. I. Cook et al., 2016; Steiger et al., 2019; Stevenson et al., 2016). The first approach uses general circulation models (GCMs) of varying degrees of complexity to simulate fluctuations in the ocean and atmosphere that may lead to megadrought in millennial-scale simulations (e.g., Coats et al., 2015; Hunt, 2006; Stevenson et al., 2015, 2018). The advantage of this approach is that it links prolonged droughts to

their physical and dynamical causes in the climate system. However, there are a few critical drawbacks with this approach when evaluating the possibility that an unusual sequence of La Niña events could cause megadroughts. First, GCMs do not always reproduce observed teleconnections between the tropical Pacific and the western US (Carrillo et al., 2018; Coats, Smerdom, Seager, et al., 2013), nor do their teleconnection strengths remain stable on multicentury timescales (Coats, Smerdon, Cook, et al., 2013). Second, GCMs often simulate El Niño–Southern Oscillation (ENSO) variations that are too frequent and too energetic on interannual timescales (e.g., Ault et al., 2013; Guilyardi et al., 2009); this too energetic ENSO variability, in turn, makes it extremely unlikely that any given simulation will see an "unusual" sequence of La Niña events because the tropical Pacific frequently switches states between relatively strong La Niña and El Niño conditions. Finally, the simulations to-date using GCMs to characterize megadroughts use either a fully couple global ocean, which makes it impossible to isolate the effects of the tropical Pacific on megadrought statistics, or an atmosphere-only model with climatological sea surface temperatures (SSTs; e.g., Stevenson et al., 2015), which does not include El Niño and La Niña variations.

As an alternative to the GCM-based approach to characterizing megadrought, several studies have developed statistical models of drought using SST anomalies based on empirical relationships (e.g., Ault et al., 2018; Coats, Smerdom, Seager, et al., 2013; Coats et al., 2015). For example, using a linear inverse model (LIM) of internal climate variability, Ault et al. (2018) found that the frequency, magnitude, and spatial scale of megadroughts during the last millennium are consistent with the statistics of an unforced climate system. While Ault et al. (2018) established a "robust" null hypothesis for the occurrence of megadrought in the western US, the study was not designed to simulate the dynamic circulation patterns in the atmosphere. Moreover, the authors employed a LIM with nearly global SST anomalies, meaning that the statistical relationships responsible for pushing the western US into megadrought could originate from high-latitude sources of low-frequency variability (e.g., the Atlantic Multidecadal Oscillation or the Pacific Decadal Oscillation).

From the defined four characteristics—frequency, magnitude, spatial scale, and mean-shift—that could classify megadroughts (Ault et al., 2018), the mean-shift of the climate during the Medieval Climate Anomaly (MCA) era is a key component for the predominant clustering of megadrought (Coats et al., 2016). In other words, during the MCA, intensification of droughts is not possible if the mean-shift is artificially removed. Attempts to identify the cause of this clustering remains inconclusive (Ault et al., 2018; Coats et al., 2016). This opens the question whether the mean-shift is due to low-frequency variability in the Pacific or Atlantic. New global climate reconstructions (e.g., the Paleo Hydrodynamics Data Assimilation, PHYDA; Steiger et al., 2019, 2021) or synthetic climate simulation, as we propose here, can aid exploration of the role of low-frequency climate variability in the MCA climate shift and its importance for the documented megadrought clustering.

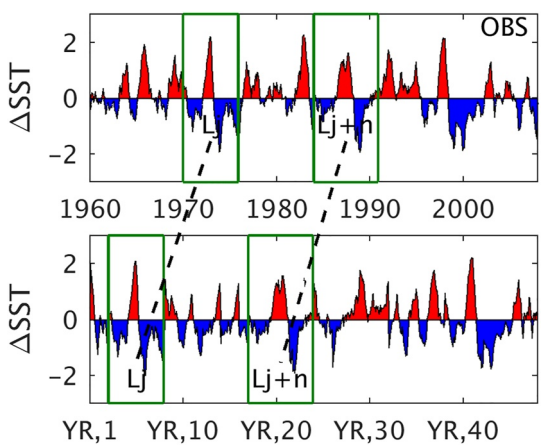

Figure 1. El Niño 3.4 time series to illustrate the moving-blocks bootstrap (mv-Ba) methodology. The upper plot is the observational (OBS), original NINO3.4 sea surface temperature (SST) used as the database for constructing the synthetic moving-blocks bootstrap SST. An example one realization moving-blocks bootstrap approach is shown in the lower plot for 57 years and the *x*-axis labeled in blocks of 10 years (YR). The green boxes show the construction for two moving-blocks bootstrap of different lengths that are highlighted as an example and labeled as Lj and Lj + n.

Here, we test whether or not the tropical Pacific alone could generate megadroughts by using a bootstrap methodology to construct a synthetic SST forcing field with realistic sequences of El Niño and La Niña events. We evaluate how well the method satisfies a series of criteria for realistic SST patterns and ENSO evolution. We then use these synthetic SST to drive an atmospheric model, allowing us to determine whether an inherently random series of interannual SST variations, along with internal atmospheric variability, could produce megadroughts in the SWUS.

2. Methods and Data Sets

2.1. Experimental Design

2.1.1. Constructed Synthetic SST

The key component of our experimental design is the construction of a 1,000-year-long synthetic SST data sets. Our synthetic SST should preserve four characteristics of the historical record: (a) the ENSO signature in the power spectrum at the interannual scale; (b) the spatial patterns of SST anomalies to ensure that the SST forcing for the atmospheric component in the model is realistic; (c) the seasonal cycle of SST anomalies, so ENSO peaks in boreal winter; and (d) the evolution of the ENSO cycle with transi-

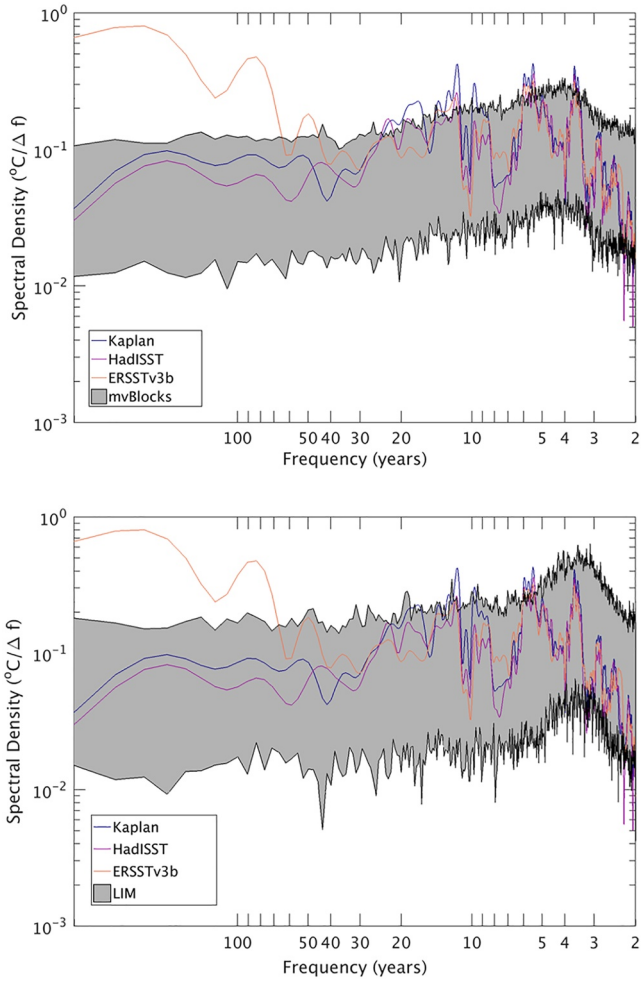

Figure 2. (top) Upper and low 95% confidence limits of NINO3.4 power spectra computed from 100 stochastically generated moving-blocks bootstrap realizations (confidence limits shown in gray shading), and three different observational sea surface temperature (SST) data products: Kaplan, HadISST, and ERSSTv3b. (bottom) Same analysis as top panel but for SST constructed with the linear inverse model (LIM).

tions from El Niño to La Niña embedded in the SST forcing fields. Therefore, the millennial synthetic SST field should isolate interannual variability in a long simulation to answer whether megadroughts can be generated as part of the natural variability without requiring an external forcing such as solar irradiance, volcanic eruptions, or orbital trends. This allows us to answer whether the bootstrap method produces realistic teleconnections between the tropical Pacific and terrestrial hydroclimate when coupled to a GCM.

2.1.2. Low-Frequency Signal in the SST

As a first step, we removed the observed linear trend in the SST before doing the sampling for the calculation of the synthetic SST with a moving-blocks approach (described below). The correction was done over the length of the observational period: 1960–2010. Although the trend is small in the tropics, the mv-Ba model would exhibit a low-frequency SST signal due to the long sampling of the observed historical trend (Mann et al., 2009). We used a linear regression method because it does not change the statistics of the SST with the mv-Ba approach. Thus, the regression approach removes the global net radiative force-like term (Mann et al., 2009) obtained from surface temperature (HadCRUT4; Osborn & Jones, 2014). First, we computed a global average surface temperature. Second, we removed the seasonality on the global surface temperature and then smoothed it using a 10-year running-mean filter (Figure S1a in Supporting Information S1). Third, we applied a linear regression of this global surface temperature to fit SST data at each grid point (see the example for one grid point in the tropics in Figure S1b in Supporting Information S1). This is done to estimate the amplitude of the low-frequency signal (trend-like), which differs at every grid point and to avoid removing SST variability in the interannual timescale. Finally, we did the correction by subtracting this adjusted trend (Figure S1c in Supporting Information S1).

2.1.3. Moving-Blocks Bootstrap Approach for Constructing SST

After removing the low-frequency variability, the generated synthetic SST uses a moving-blocks (mv-Ba) bootstrap approach (Wilks, 1997). In general, a bootstrap data generation emulates the statistics of a system by resampling a collection of a short original data set (Wilks, 2011). In the moving-blocks bootstrap approach, randomization is done in blocks to preserve the seasonal evolution of ENSO but destroys any autocorrelation on low-frequency timescales. The resampling is done over a variable length segment of the original data that is defined by the duration of ENSO (Figure 1), with the specific goal of retaining ENSO-like variability. Two constraints were used to guarantee conservation of seasonality and smooth continuity within the final time series. First, the default length of the mv-Ba bootstrap is 12 months for neutral years and variable for ENSO years (random between 2 and 7). As the SST was randomly sampled by year, there is no continuity from December to January. We have not explored the impact of this in the GCM simulation, however, as the discontinuity only happens for the neutral years, the impact on El Niño or La Niña events is irrelevant. Second, whenever the selected year is into an El Niño or La Niña phase, we use the complete cycle of the event. As these events do not start in January nor end in December, we extended its original cycle length with random values, so it always runs for an entire year. The random SST values were taken from the neutral years, so there were no abrupt changes from year-to-year sampling. The beginning and end of the El Niño (La Niña) cycle were defined by a threshold of 0.5 units of SST from the 3-month running mean. The bootstrap sampling process is done with the Niño 3.4 index (Trenberth, 1997) as reference, so we have the original sequence of El Niño and La Niña events with the block construction over the total SST field. To generate the synthetic SST, monthly observational data from the period 1960–2007 is used as a sampling pool, and it is resampled with reordering. As a result, we get a different sequence of El Niño and La Niña events that is completely analogous to what occurred in the historical period. Historical SST data for this resampling originate from the NOAA extended reconstructed SST (ERSST; Smith et al., 2008).

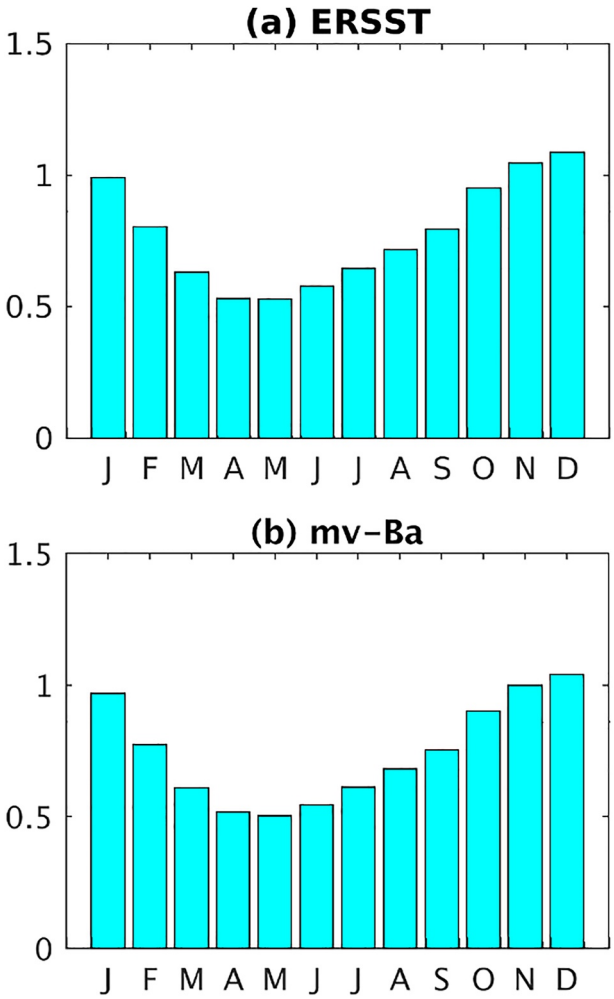

Figure 3. Monthly standard deviation for NINO3.4 region from (a) observations from the extended reconstructed sea surface temperature (ERSST) and (b) the moving-blocks bootstrap (mv-Ba) statistical approach employed here.

2.1.4. The Linear Inverse Model of SST

As in Ault et al. (2018), we used a LIM approach as a benchmark to compare against the result with mv-Ba, but the alternative millennial SST from LIM is not used in the CAM5 experiment (see next). The LIM generates "multivariate red noise," which is analogous to a first-order autoregressive (AR(1)) process; commonly used to test the null hypothesis for a unidimensional time series such as $\frac{dX}{dt} = LX + \zeta$. In LIM, autocorrelation coefficients are constructed with a linear deterministic feedback metric (L), and we use a multidimensional field (X) instead of a unidimensional time series. In this framework, we define X with three fields: SST, sea surface height, and the Palmer drought severity index (PDSI; Palmer, 1965). ζ is the stochastic white noise forcing, which generates the variance that perturbs the linear system. For further details see Ault et al. (2018).

2.1.5. The Tropical–Extratropical Transition Zones

The synthetic SSTs are defined only in the tropical domain for both the mv-Ba SST and LIM SST between 20°S and 20°N (Figure S2 in Supporting Information S1). Next, the tropical SST is merged with a climatological SST (annual cycle) from ±35° to the poles using the same data originally used to obtain the SST. Finally, the regions between 20°N and 35°N and 20°S–35°S are linearly interpolated to reduce abrupt transitions from the tropics to the extratropics. This restriction is important because internal variability might play an important role in megadrought development during decadal and centennial scales (Coats et al., 2015).

2.2. The Community Atmosphere Model

The SST generated with the mv-Ba procedure is used to force the Community Atmospheric Model version 5 (CAM5). Our CAM5 simulation is a 1,000-year-long run with the mv-Ba SST (CAM5-mv-Ba). To the extent possible, our simulation follows a similar experimental design to the control runs in the Last Millennium Ensemble (LME; Otto-Bliesner et al., 2016). Our CAM5 simulation used prescribed SST in the tropics between 20°S and 20°N as in the Tropical Ocean-Global Atmosphere (TOGA) experiments (Deser et al., 2017; Gates et al., 1998; Hurrell et al., 2008; Phillips, 1996; Webster & Lukas, 1992). We also use fixed ice configuration (Rayner et al., 2003), with 1980–2007 climatological ice concentration. Both SST and ice are interpolated in time to center the data at the middle of each month (Taylor et al., 2000). Total solar irradiance and orbital parameters are fixed to the year 850 CE for the entire run. CAM5 is used under the modeling framework of the Community Earth System Model (CESM; Hurell et al., 2013) version 1.2.2 with 30 vertical levels in the atmosphere (from the surface to 2 mb) and 15 soil levels (from the surface to 35 m underground). The horizontal resolution for this experiment is 1.9° × 2.5° with the finite volume dynamical core (Lin & Rood, 1997).

2.3. The Palmer Drought Severity Index

The PSDI was calculated from several sources: from the North American Drought Atlas (NADA; E. R. Cook et al., 2010), from the LIM using observations (Ault et al., 2018), from the CESM-LE, from mv-Ba, and from CESM-mv-Ba. PDSI has been used since the 1960s to evaluate droughts across the U.S. and worldwide (Palmer, 1965). The PDSI was computed using the Thornthwaite (TH) and Penman–Monteith (PM) variations for the potential evapotranspiration (van der Schrier et al., 2011). To compute potential evapotranspiration needed for the water budget balance in PDSI, we use net radiation fields from the NCEP/NCAR Reanalysis 1 (Kalnay et al., 1996) and model outputs from CESM.

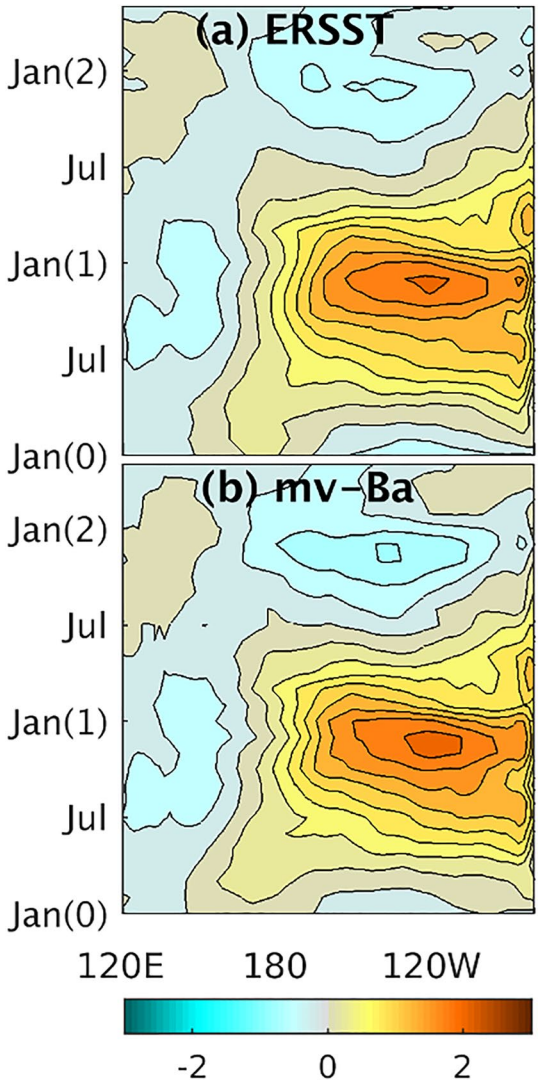

Figure 4. Hovmoller diagrams of seasonal evolution of tropical [5°S–5°N] sea surface temperature (SST) anomaly for two data sets: (a) the extended reconstructed SST (ERSST) and (b) the moving-blocks bootstrap (mv-Ba) SST. The diagrams are composite for El Niño events identified in these databases for its entire life cycle starting in January of the onset year, Jan(0), and ending 2 years after, Jan(2).

The NADA PDSI used tree-ring chronologies for its construction, and it was taken from the NOAA paleoclimate archive. For the LIM, we used a PDSI and SST computed with observational record (1960–2007) to feed a LIM model in the same way done in Ault et al. (2018). For both CESM (LE and mv-Ba), the PDSI is constructed with the needed input (precipitation, temperature, radiation fields, surface pressure, and humidity) from the modeling outputs. For the mv-Ba PDSI, the PDSI is constructed with the bootstrapped SST sequence applied on the atmospheric variables (precipitation, temperature, etc.). The calibration period for these PDSIs is not the same in all the cases, and that is a caveat in the result we have presented. However, in the historical period, our PDSI was compared with NOAA's PDSI (Dai et al., 2004), and its analysis shows that the signal of drought exists in both data sets. Although NOAA's PDSI has different calibration period, a numerical comparation for the Southwest region shows that both data sets share an explained variance of 77.4%.

2.4. Statistical Characteristics of Megadrought

While the mv-Ba statistical model can be run hundreds of times for thousands of years, CAM5 was simulated only for 1,000 years. We therefore run large numbers of realizations of the mv-Ba model, then examine the distributions of key statistics that describe the power spectrum, seasonality, and spatial patterns of tropical Pacific SST variability in these oceans. To identify megadroughts in our mv-Ba realizations, we use the same metrics as Ault et al. (2018): magnitude, spatial scale, clustering of events, and shift of the mean. The magnitude is defined by the minimum PDSI in the record. Specifically, we compute the 35-year running mean of PDSI ($PDSI_{35}$) from both reconstructions and model data, then use its minimum values over a 1,000-year period to identify the "worst" prolonged event. To characterize the spatial scale of megadroughts in the western US, we calculate the fraction of the domain with $PDSI_{35}$ values below −1 standard deviation. This fraction is then used as a drought area index (DAI). Clustering of events refer to megadroughts happening in the first 500 years of the reconstructed record. The shift of the mean is any significant change of the mean $PDSI_{35}$ between the early and late 500-year period.

In the present study, the significance testing of our claim was tested with nonparametric distributions using the five steps of the hypothesis test (Wilks, 2011): (a) the test statistic distribution of each megadrought characteristic is obtained using LIM over the data set ($PDSI_{35}$ and DAI_{35}) from the CAM5-mv-Ba simulation (run with the SST constructed with random ENSO); (b) the null distribution, *Ho* (we hope to reject), is a nonparametric probability density function (PDF) using LIM, but this distribution is obtained by randomizing the sequence of the data set from the CAM5-mv-Ba simulation (i.e., limiting the opportunity of consecutive ENSO in every resampling of the control simulation); (c) the alternative hypothesis, H_A, is just that *Ho* is not true; (d) the null distribution is obtained as described above; and (e) we compare distributions, if the test statistic distribution fall in the sufficient improbable region of *Ho*, then *Ho* is rejected. As in our previous study, the null hypothesis for clustering of events and shift of the mean were not rejected and we cannot claim that clustering and shift of mean occur from internal and ENSO-like variability only, and therefore our conclusions are the same for these two parameters. PDFs are computed using each of these test statistics from the mv-Ba statistical model and compared against observations and new simulations.

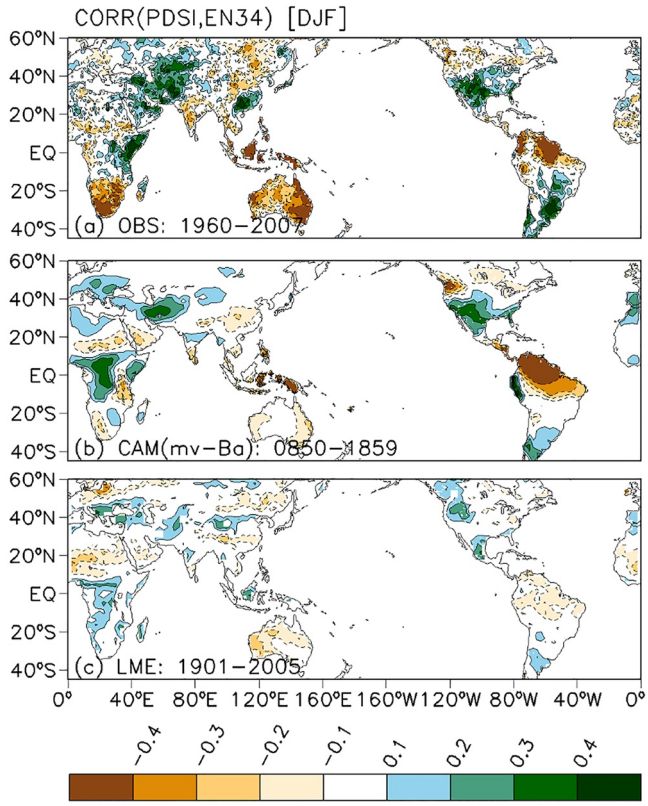

Figure 5. Correlation winter patterns (December–January–February, DJF) between El Niño 3.4 sea surface temperature (SST) and Palmer drought severity index (PDSI) for four databases: (a) observational data from the extended reconstructed SST and PDSI from Sheffield et al. (2012); (b) SST and PDSI obtained from a CAM simulation driven with SST randomly obtained from the moving-blocks bootstrap approach, CAM(mv-Ba); and (c) SST and PDSI obtained from a simulation from the Last Millennium Ensemble (LME).

2.5. The LME Experiment

We use the rich archive of model outputs from the LME experiment (Otto-Bliesner et al., 2016), which are a set of simulations all based on the CESM with CAM5 as an atmospheric model. The LME experiment has the primary goal of exploring sources of uncertainty in the reconstruction of the external forcing that drives the climate of the past millennium. Here, the purpose is to check the skill of CAM5 (with LME and the CAM5-mv-Ba millennial simulation) to capture drought variability in the SWUS. We further investigate whether the drought pattern in the CAM5-mv-Ba simulation is comparable with the LME CAM5. In this study, we used 35 LME simulations. We used these multiple agents to generate an approximation of the most probable scenario with several forcing simulations: volcanic eruption, changes in solar irradiance, orbital, greenhouse gas level, land use-land cover, and the full forcing. In our analysis, we did not make a distinction among the external forcing. The LME includes ensemble members with random perturbations of the order of 10^{-14}°C in the air temperature field at the initialization of the simulation. We employed the first 1,000 years from each simulation (850–1849) to avoid the postindustrial global warming era and also including industrial climate record for comparisons with observation (1901–2005).

3. Results

3.1. Statistical Characteristics of Mv-Ba Tropical SSTs

Do the mv-Ba statistical SST emulators preserve the power spectrum of ENSO on interannual timescales? The distribution of NINO3.4 power spectra generated by the mv-Ba statistical model is consistent with the characteristics of interannual variability in the tropics (Figure 2) and similar to the LIM. Using 100 realizations (a total of 100,000 years) from mv-Ba and LIM, both approaches can reproduce the observed spectral peaks at the interannual range (x-axis < 10 years) at the 95% confidence level. Specifically, the spectral density of the mv-Ba approach fully encompasses the range of spectral densities recorded in observational data sets across 2-year to 7-year frequencies (gray shading, Figure 2). On interdecadal timescale (x-axis > 10 years), spectral amplitude of both distributions decreases. Consequently, these attributes of the mv-Ba ensure that high amplitude, low-frequency (decadal- to century-scale) variability is not present in the SST forcing fields we later couple to CAM5.

Do our statistical SST fields exhibit realistic spatial patterns of tropical Pacific anomalies? The annual spatial pattern of variance in SST generated by mv-Ba is close to the one seen in observations (Figure S3 in Supporting Information S1). The major variability occurs in the eastern Pacific Ocean. With this result, we can claim that at the annual scale the approach is comparable from observations, which will explain later the convergence of the drought results at the long-term run in the CAM5 simulation. However, analyzing the variance at monthly scale, greater similarity exists within the mv-Ba results. The seasonal amplitude of variance in the NINO3.4 region in the mv-Ba distribution is virtually identical to observations (Figure 3), as the variance is coming from the bootstrap approach.

Do our statistical methods reproduce the seasonal cycle of SST variance and ENSO evolution? The mv-Ba approach resolves seasonality well, which does not require El Niño (and La Niña) events to be phase-locked to the annual cycle. As a result, applying mv-Ba to SST allows a realistic seasonal evolution of ENSO in the tropics (Figure 4). Using moving blocks, we see transitions from El Niño to La Niña phase that peak in January of the El Niño year that are very similar to transitions seen in observed ENSO years. As in the observations (and in the mv-Ba approach), La Niña events tend to follow El Niño events. Nevertheless, the mv-Ba (by construction) does

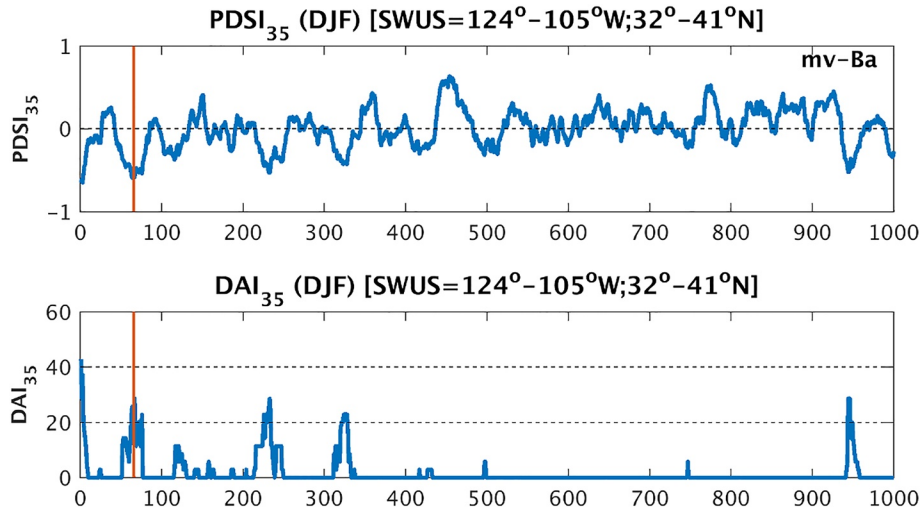

Figure 6. Palmer drought severity index (PSDI) and drought area index (DAI) time series defined over the SWUS region (124°–105°W and 32°–41°N) from the CAM5-mv-Ba simulation with sea surface temperature (SST) generated by the moving-block (mv-Ba) bootstrap approach, showing one candidate for megadrought events (DAI > 20%) as highlighted with the vertical solid line. The PDSI and DAI time series were smoothed with a 35-year running-mean average filter, $PDSI_{35}$ and DAI_{35}.

overall well at reproducing the observed seasonality of SSTs in the tropical Pacific, the phase locking of El Niño and La Niña events with the annual cycle, and the seasonal evolution of individual events.

Does the mv-Ba method reproduce realistic statistics of teleconnections between the tropical Pacific and terrestrial hydroclimate when coupled to CAM5? A correlation analysis between mv-Ba tropical SST (for El Niño 3.4 region) and statistically generated PDSI shows the typical opposite-sign PDSI pattern between the SWUS hydroclimate and the Pacific Northwest variability (Figure S4 in Supporting Information S1). A positive relationship between PDSI, within the SWUS, and El Niño 3.4 is evident in different realizations of the statistical climate. Several CESM simulations have shown a significant correlation between SST and PDSI. These findings are consistent with SST and PDSI from instrumental records (Figure 5). Surprisingly, the variability of PDSI from CAM5-mv-Ba is consistent with observations, and it exhibits a more coherent pattern than the fully coupled LME simulations. We suggest these matching patterns as evidence that key hydroclimate variability in the SWUS originates from the tropical climate variability (Coats, Smerdom, Seager, et al., 2013). Since the LME is a fully coupled simulation, this difference to observations and the CESM-vs-Ba simulations might be due to the fixed SST forcing, or perhaps the lack of accuracy in the LME ocean–atmosphere coupling simulations.

3.2. Megadroughts in a Hybrid Simulation

Equipped with a better understanding of the statistical behavior of the mv-Ba statistical SST generator, we now turn to our experiment where we couple one realization from the model to CAM5. In just one CAM5 run of 1,000-year presampled observations, there is an event (DAI_{35} > 20%) as severe as the most severe event ($DAI_{35} \approx 40\%$; Ault et al., 2018) of the last millennium in the observation-based reconstructed PDSI for the SWUS (Figures 6 and 7). Spatial patterns of drought metrics produced by CAM5-mv-Ba look as realistic as those in the observed paleoclimate records (Figure 5). Both PDSI and DAI identify megadrought in the simulated 1,000-year record (Figure 6). The DAI measures the percentage of the domain under drought conditions (PDSI < −1 units). Composite analysis of these drought metrics for two different data sets, the mv-Ba SST and CAM5-mv-Ba SST, supports our working hypothesis that megadroughts occur in both the stochastic (Figure S5 in Supporting Information S1) and the dynamically generated climate states (Figure 7). This analysis suggests that tropical SST variability can drive megadrought based on random processes via the correct large-scale teleconnection. A composite analysis of SST_{35} (a 35-year running-mean filter of SST; Figure 7 and Figure S4 in Supporting Information S1; bottom) and a correlation analysis (Figure S6 in Supporting Information S1) during megadroughts in SWUS show a predominant La Niña-like pattern, as La Niña has been linked to dry conditions in the SWUS (Herweijer et al., 2007; Seager et al., 2005), which is also observed in the LME experiment but with

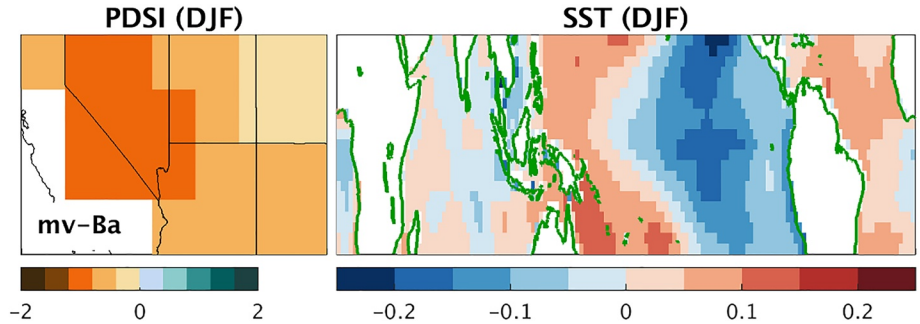

Figure 7. Palmer drought severity index (PSDI) and sea surface temperature (SST) for a megadrought case using a CAM5 simulation for the moving-block (mv-Ba) approach. The case is the one identified in Figure 6, so the panels are the average fields over 35 years that defined the megadrought duration indicated by the vertical line in the DAI_{35} time series.

a minor impact over land (Figure 8) and a weak ocean teleconnection (Figure 9). Results from our previous work using LIM (i.e., Ault et al., 2018) are also consistent with this analysis, and they suggest a similar mechanism. However, this study did not explore the impact of different flavors of ENSO (central Pacific, eastern Pacific, etc.) on megadrought in the US southwest.

3.3. Megadrought Statistics

The hybrid modeling approach (CAM5-mv-Ba) confirms the statistically significant occurrence of megadrought in the SWUS similar to paleoclimate records and LIM (Figure 10). Results from CAM5-mv-Ba are compared with the PDF of several LIM runs used as benchmark (cyan histogram in Figure 10). As in Ault et al. (2018), we computed megadrought characteristics for the SWUS: (a) magnitude and (b) spatial scale. Comparing the test statistic to the null distribution for the magnitude and spatial scale, *Ho* were rejected at the 95% confidence level (as noted by the dark gray null distribution in Figure 10), meaning that both the magnitude and spatial scale of megadroughts are statistically significant in this experiment. Therefore, megadroughts—as defined by their magnitude and spatial scale—may occur by internal climate variability and random La Niña-like SST pattern and not random climate variability.

3.3.1. The Magnitude of Megadrought: $PDSI_{35}$

The drought magnitude statistic is defined by the PDF in the cyan histogram with LIM (Figure 10a), whose $PDSI_{35}$ mean is −0.6. This cyan histogram represents the minimum $PDSI_{35}$ value over a 1,000-year time series with a total pool of 1,000 samples taken from the LIM. We obtained the primary sample pool from the 1,000-year CAM5-mv-Ba run. The secondary sample pool was generated by resampling a 100-year time series of both the PDSI and the SST from the same CAM5-mv-Ba run, then using a LIM to stochastically generate a new 1,000-year stochastic $PDSI_{35}$ (Ault et al., 2018). The $PDSI_{35}$ with marks (*, ×, and + in Figure 10a) are computed using data sets from the NADA (E. R. Cook et al., 2010) and the CAM5-mv-Ba bootstrap. From these three data sets, the NADA $PDSI_{35}$ is the driest event. PDSI was computed from CAM5-mv-Ba (fix SST-forced) once the simulation generated the moisture anomalies in the SWUS. This analysis shows that megadrought magnitude observed in tree-ring chronology is part of the LIM-PDSI distribution based on CAM5-mv-Ba at the 95% confidence level (indicated by the light gray region). The null hypothesis, *Ho*, of the magnitude is that this parameter can rise from a random process of climate variability that does not include a series of random La Niña events. In Figure 10, the dark gray histogram shows its null distribution, and therefore we can reject *Ho*. The null distribution was generated by randomizing the sequence of each 1,000-year PDSI time series pool of 1,000 samples from the CESM-mv-Ba run. The parameter distribution shows that the NADA megadrought intensity during the MCA is not an extreme case, but one that is in 90% (probability of $PDSI_{35}$ be more intense than the case measured in NADA, $Pr\{X \leq x(NADA)\} = 0.9$ from Figure 10a) of the "classical" megadrought. Therefore, megadrought of higher intensity than the one found in the paleoclimate tree-ring record is possible and could happen in the future.

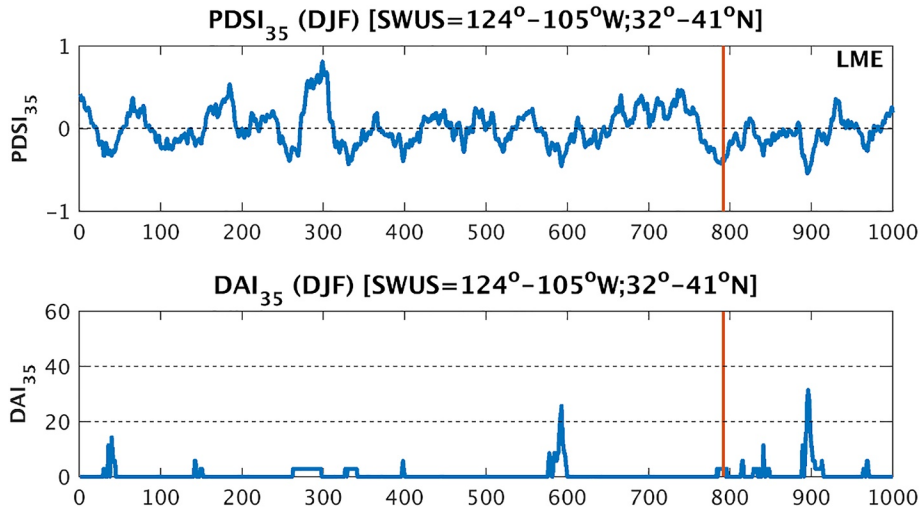

Figure 8. Palmer drought severity index (PSDI) and drought area index (DAI) time series defined over the SWUS region (124°–105°W and 32°–41°N) that shows one poor candidate for megadrought events (DAI < 20% but PDSI < −0.5) as highlighted with the vertical solid line. The PDSI and DAI time series were smoothed with a 35-year running-mean average filter, $PDSI_{35}$ and DAI_{35}. These time series correspond to the first millennium of the Last Millennium Ensemble (LME) experiment.

3.3.2. The Spatial Scale of Megadrought: DAI_{35}

The spatial scale of megadrought in the SWUS also shows statistically significant results (Figure 10b). For this, we use a slightly different approach from Ault et al. (2018), but with similar conclusions. Here, we introduce the scaled drought area index, scaled-DAI_{35} = $PDSI_{35}$ × DAI_{35}, because it conserves the DAI against different PDSI thresholds. As DAI_{35} and $PDSI_{35}$ for the SWUS have an inverse linear relationship for extreme values (Figure S7 in Supporting Information S1), analyzing DAI_{35} using different area thresholds makes analysis not generalized. However, scaling DAI (by multiplying it by its PDSI value) eliminates values that are not relevant for megadrought statistics, for example, values close to zero for both PDSI and DAI. Therefore, the scaled-DAI_{35} provides a generalized parameter that is conservative along different PDSI thresholds that are used to compute DAI. As noted in Supporting Information S1, the peak of the scaled-DAI_{35} distribution is near the same value (e.g., −15 scaled-DAI_{35} units) for different PDSI thresholds (Figure S8 in Supporting Information S1). Therefore, scaled-DAI_{35} is conservative against changes of PDSI. Using this new scaled-DAI_{35} distribution (Figure 10b), we show that megadrought spatial scale as computed with tree-ring chronologies (NADA), mv-Ba, and CAM5-mv-Ba is part of the same statistically dynamically generated pool of megadrought distribution (cyan histogram) and significantly different from the random realization (dark gray histogram).

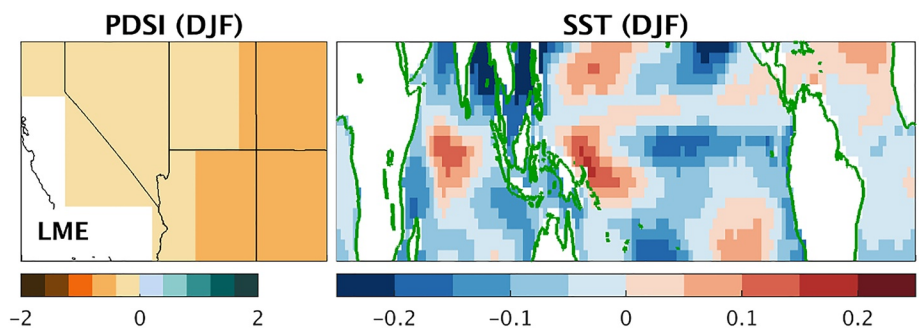

Figure 9. Palmer drought severity index (PSDI) and sea surface temperature (SST) for a megadrought case using a simulation of the Last Millennium Ensemble (LME) experiment. The case is the one identified in Figure 8, so the panels are the average fields over 35 years that defined the megadrought duration indicated by the vertical line in the DAI_{35} time series.

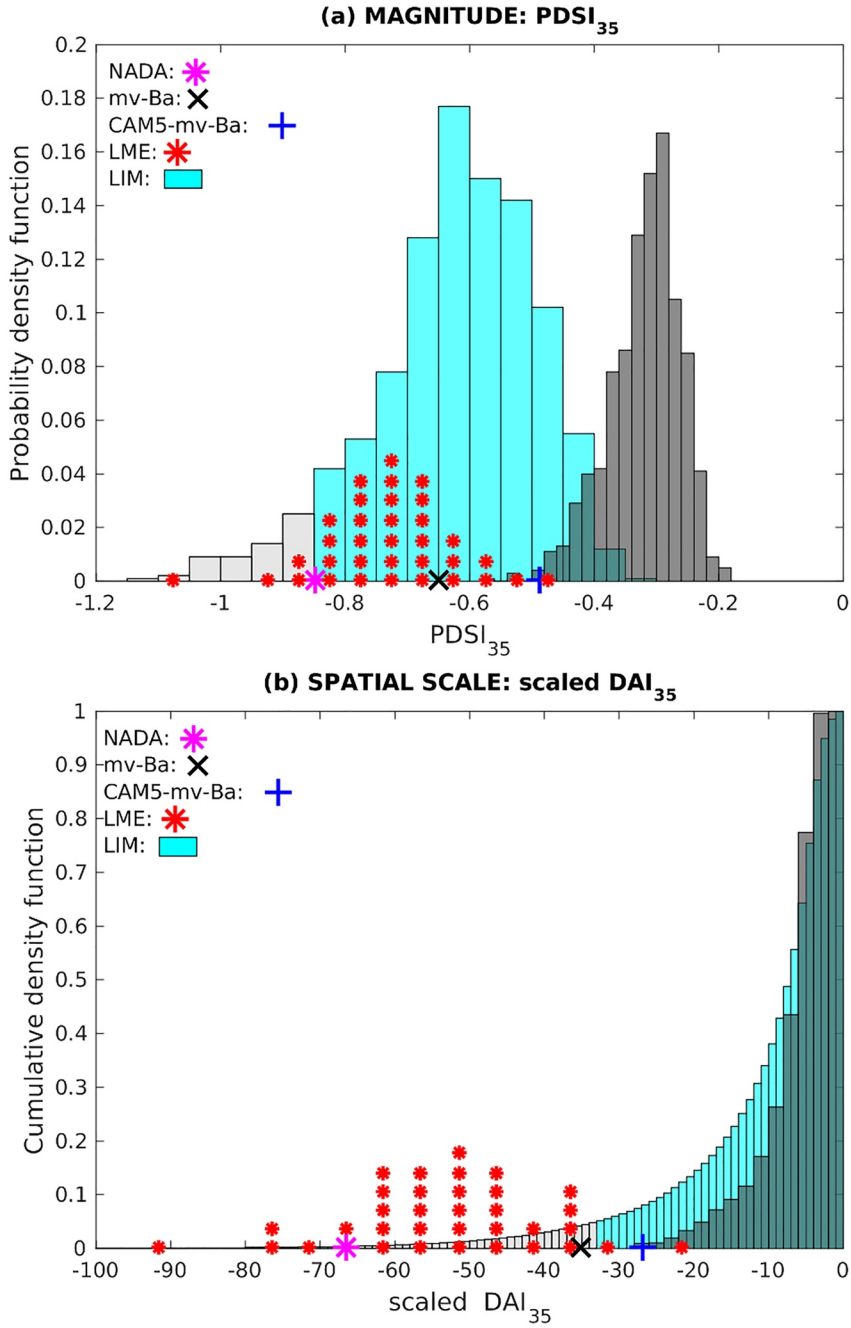

Figure 10. Probability density function (PDF) of the megadrought magnitude (a) and cumulative density function (CDF) of megadrought spatial scale (b). The megadrought magnitude (parameter) is defined by the minimum of the Palmer drought severity index (PDSI) in a 1,000-year time series. The megadrought spatial scale (parameter) is defined by the scaled drought area index, scaled-DAI_{35}. All the 1,000-year time series used a running-mean average over 35 years ($PDSI_{35}$) and are defined over the Southwestern US (SWUS: 124°–105°W and 32°–41°N). Three sources of data are presented. (a) The cyan-colored histograms (PDF and CDF) are computed using LIM 1,000 times over the CAM5-mv-Ba millennial run. In other words, it uses two data pools. The primary sample pool is from the 1,000-year CAM5-mv-Ba run. The secondary sample pools were generated by resampling the CAM5-mv-Ba 1,000 times (a resampling uses a 100-year time series of both the PDSI and SST), and then using the LIM to stochastically generate a 1,000-year $PDSI_{35}$ (Ault et al., 2018). (b) The three colored marks (*, ×, and +) are the $PDSI_{35}$ magnitude and DAI_{35} spatial scale computed with three different data sets: NADA, mv-Ba, and CAM5-mv-Ba; all with a 1,000-year record length. (c) The red dots are the $PDSI_{35}$ magnitude and DAI_{35} spatial scale computed with 35 simulations from the Last Millennium Ensemble (LME) experiment. Each red dot represents one simulation, so they are plotted using a histogram style. The dark gray histograms (PDF and CDF) are the null distributions. The null distribution is generated by randomizing the sequence of each 1,000-year time series ($PDSI_{35}$ and scaled-DAI_{35}) in the secondary pool (of 1,000 samples) originated from the CESM-mv-Ba run. The 95% confidence level is indicated by the light gray region.

4. Conclusions

Our experiments show that SWUS megadroughts are not conditionally linked to low-frequency variability in the tropical Pacific. A synthetic tropical SST is constructed to test the significance of megadrought occurrence driven by a series of La Niña events. This synthetic SST is stochastically sampled from the current climate (1960–present) but detrended to reduce observed warming trend signals. We sampled observations focusing on interannual rather than decadal or centennial SST variability. Still, our approach preserves the power spectrum, seasonal cycle, spatial pattern, and ENSO evolution. The so constructed synthetic SSTs are used to drive an atmospheric model. The resulting climate reproduces megadrought statistics similar to those achieved in the stochastic LIM of Ault et al. (2018). With respect to a robust null hypothesis test, this study claims that the spatial scale and magnitude of megadrought in the SWUS can be generated from natural variability of the interannual climate regime. This provides additional evidence that decadal variability could arise from internal variability at the interannual scale (Newman et al., 2016). In addition, our experiment isolates any potential low-frequency variability in the Atlantic Ocean, though we acknowledged that during megadroughts in the CAM5 mv-Ba, the Atlantic SSTs tend to be relatively warm. Also, our experiment shows that SW megadrought is not exclusively driven by low-frequency variability in the tropical Pacific. For paleoclimate research, our approach can help to test the significance of the low-frequency signals in the tree-ring chronologies, as this approach merges statistical knowledge of the current climate with an extension of potential synthetic climate scenarios.

The CAM5 hybrid setting seems to properly simulate megadroughts in the SWUS, even at a relatively coarse spatial resolution. As speculated in Coats, Smerdom, Seager, et al. (2013), both stochastic atmospheric variability and ENSO are capable of producing megadrought in the SWUS. However, further investigation is required to determine whether internal atmospheric variability alone can generate 35-year droughts, and not just shorter 15-year megadrought (Stevenson et al., 2015). For climate change projections, the presented results motivate further exploration of this hybrid modeling framework to evaluate the impact of external forcing: solar irradiance, volcanic eruptions, and orbital trends. The PDSI (calculated from CAM5-mv-Ba) analysis validates the previous finding of megadrought characteristics using the stochastic LIM approach (Ault et al., 2018). Composite and spectral analyses of SST and PDSI show strong teleconnection patterns in observations and CAM5-mv-Ba, something not seen in a fully coupled LME simulation (Landrum et al., 2013; Mann et al., 2009), which supports the legitimacy of our experimental setup. Previous work (Ault et al., 2018) shows that the worst event described in the NADA is not significantly different from the LIM-based null hypothesis. The worst event in the mv-Ba bootstrap experiment is also consistent with that null hypothesis.

In particular, megadroughts in the Southwest appear to have "clustered" around the MCA. State-of-the art model simulations do not reproduce that clustering, nor do they simulate the MCA as being drier on average than more recent centuries (e.g., Coats et al., 2016). Two of these paleoclimate-derived megadrought statistics (clustering and mean-shift) were not reproduced by our experiment. This expected result motivates the implementation of additional experiments. We will use the CAM5 to conduct new experiments with idealized forcings of dust, SSTs, solar forcing, and land-surface feedbacks to investigate whether this increases megadrought clustering or leads to mean climate drying over the region, as during the MCA. However, the study here shows that even absent unexplored feedbacks, external forcings, or low-frequency Pacific variability, the risk for megadroughts is omnipresent in today's climate, as all they require is an unfortunate series of La Niña events.

Data Availability Statement

[Software]: The CESM model was provided by NCAR-UCAR: https://www.cesm.ucar.edu/models/ (Hurell et al., 2013) and used to create the millennial CAM5-mv-Ba simulation in this manuscript. [Access condition]: The NCAR computational facilities were used to perform the CAM5-mv-Ba simulation under grant UCOR0018. [Data]: The Last Millennium Ensemble (LME) data set is from the CESM Paleoclimate Working Group at NCAR and available via the Climate Data Gateway at NCAR: http://www.earthsystemgrid.org (Otto-Bliesner et al., 2016). [Data]: The global surface temperature was obtained from the Met Office Hadley Center at https://www.metoffice.gov.uk/hadobs/hadcrut4/data/current/time_series/HadCRUT.4.6.0.0.monthly_ns_avg.txt (HadCRUT4; Osborn & Jones, 2014). [Data]: The historical sea surface temperature (SST) data set is from the NOAA extended reconstructed SST at https://www.ncei.noaa.gov/products/extended-reconstructed-sst (Smith et al., 2010). [Software]: Figures were made with Matlab version R2016a (license by the MathWorks, Inc.),

available under the Matlab academic license at https://www.mathworks.com. [Software]: Maps (Figure 5) were created through the Grid Analysis and Display System (GrADS) version 2.0.a9 (Doty, 1995) and the copyright © 1988–2010 by Brian Doty and the Institute for Global Environment and Society (IGES) now available at http://cola.gmu.edu/grads/.

Acknowledgments
The authors thank NCAR for the use of its computing facilities. The simulations were performed at the NCAR-Wyoming supercomputer. The CESM project is supported primarily by the National Science Foundation (NSF). This work was partially supported by the P2C2 NSF Grant 1602564 and CAREER NSF Grant 17535. F.L. was supported by supported by the U.S. Department of Energy, Office of Science, Office of Biological & Environmental Research (BER), Regional and Global Model Analysis (RGMA) component of the Earth and Environmental System Modeling Program under Award Number DE-SC0022070, and National Science Foundation (NSF) IA 1947282.

References

Ault, T. R., Cole, J. E., Overpeck, J. T., Pederson, G. T., George, S. S., Otto-Bliesner, B., et al. (2013). The continuum of hydroclimate variability in western North America during the last millennium. *Journal of Climate*, *26*, 5863–5878. https://doi.org/10.1175/JCLI-D-11-00732.1

Ault, T. R., Cole, J. E., Overpeck, J. T., Pederson, G. T., & Meko, D. M. (2014). Assessing the risk of persistent drought using climate model simulations and paleoclimate data. *Journal of Climate*, *27*, 7529–7549. https://doi.org/10.1175/JCLI-D-12-00282.1

Ault, T. R., & George, S. S. (2018). Unraveling the mysteries of megadrought. *Physics Today*, *71*, 44–50. https://doi.org/10.1063/pt.3.3997

Ault, T. R., George, S. S., Smerdon, J. E., Coats, S., Mankin, J. S., Carrillo, C. M., et al. (2018). A robust null hypothesis for the potential causes of megadrought in western North America. *Journal of Climate*, *31*, 3–24. https://doi.org/10.1175/JCLI-D-17-0154.1

Ault, T. R., Mankin, J., Cook, B. I., & Smerdon, J. E. (2016). Relative impacts of mitigation, temperature, and precipitation on 21st-century megadrought risk in the American Southwest. *Science Advances*, *2*, e1600873. https://doi.org/10.1126/sciadv.1600873

Benson, L., Petersen, K., & Stein, K. (2007). Anasazi (Pre-Columbian native-American) migrations during the middle-12th and late-13th centuries—Were they drought induced? *Journal of Climate Change*, *83*, 187–213. https://doi.org/10.1007/s10584-006-9065-y

Carrillo, C. M., Castro, C. L., Garfin, G., Chag, H. I., Bukovsky, S. M., & Mearns, L. O. (2018). Pacific sea surface temperature related influences on North American monsoon precipitation within North American Regional Climate Change Assessment Program models. *International Journal of Climatology*, *38*, 4189–4210. https://doi.org/10.1002/joc.5561

Coats, S., Smerdon, J. E., Cook, B. I., & Seager, R. (2013). Stationarity of the tropical Pacific teleconnection to North America in CMIP5/PMIP3 model simulations. *Geophysical Research Letters*, *40*, 4927–4932. https://doi.org/10.1002/grl.50938

Coats, S., Smerdon, J. E., Cook, B. I., & Seager, R. (2015). Are simulated megadroughts in the North American Southwest forced? *Journal of Climate*, *28*, 124–142. https://doi.org/10.1175/JCLI-D-14-00071.1

Coats, S., Smerdon, J. E., Karnauskas, K. B., & Seager, R. (2016). The improbable but unexceptional occurrence of megadrought clustering in the American West during the Medieval Climate Anomaly. *Environmental Research Letters*, *11*, 074025. https://doi.org/10.1088/1748-9326/11/7/074025

Coats, S., Smerdom, J. E., Seager, R., Cook, B. I., & Gonzáles-Rouco, J. F. (2013). Megadroughts in southwestern North America in ECHO-C Millennial Simulations and their comparison to proxy drought reconstruction. *Journal of Climate*, *26*, 7635–7649. https://doi.org/10.1175/JCLI-D-12-00603.1

Cook, B. I., Ault, T. R., & Smerdon, J. E. (2015). Unprecedented 21st century drought risk in the American Southwest and central plains. *Science Advances*, *1*, e1400082. https://doi.org/10.1126/sciadv.1400082

Cook, B. I., Cook, E. R., Smerdon, J. E., Seager, R., Williams, A. P., Coats, S., et al. (2016). North American megadroughts in the Common Era: Reconstructions and simulations. *Wiley Interdisciplinary Reviews Climate Change*, *7*, 411–432. https://doi.org/10.1002/wcc.394

Cook, E. R., Seager, R., Heim, R. R., Jr., Vose, R. S., Herweijer, C., & Woodhouse, C. (2010). Megadroughts in North America: Placing IPCC projections of hydroclimatic change in a long-term palaeoclimate context. *Journal of Quaternary Science*, *25*, 48–61. https://doi.org/10.1002/jqs.1303

Dai, A., Trenberth, K. E., & Qian, T. (2004). A global data set of Palmer Drought Severity Index for 1870–2002: Relationship with soil moisture and effects of surface warming. *Journal of Hydrometeorology*, *5*, 1117–1130. https://doi.org/10.1175/JHM-386.1

Deser, C., Simpson, I. R., McKinnon, K. A., & Phillips, A. S. (2017). The Northern Hemisphere extratropical atmospheric circulation response to ENSO: How well do we know it and how do we evaluate models accordingly? *Journal of Climate*, *30*, 5059–5082. https://doi.org/10.1175/JCLI-D-16-0844.1

Doty, B. (1995). The Grid Analysis and Display System (GrADS), 148. Retrieved from ftp://cola.gmu.edu/grads/beta/doc/gadoc151.pdf

Gates, W. L., Boyle, J., Covey, C., Dease, C., Doutriaux, C., Drach, R., et al. (1998). An overview of the results of the Atmospheric Model Intercomparison Project (AMIP I). *Bulletin of the American Meteorological Society*, *73*, 1962–1970.

Guilyardi, E., Braconnot, P., Jin, F.-F., Kim, S. T., Kolasinski, M., Li, T., & Musat, I. (2009). Atmosphere feedbacks during ENSO in a coupled GCM with a modified atmospheric convection scheme. *Journal of Climate*, *22*, 5698–5718. https://doi.org/10.1175/2009JCLI2815.1

Herweijer, C., Seager, R., Cook, E. R., & Emile-Geay, J. (2007). North American droughts of the last millennium form a gridded network of tree-ring data. *Journal of Climate*, *20*, 1353–1376. https://doi.org/10.1175/JCLI4042.1

Hunt, B. G. (2006). The medieval warm period, the Little Ice Age and simulated climatic variability. *Climate Dynamics*, *27*, 677–694. https://doi.org/10.1007/s00382-006-0153-5

Hurell, J., Holland, M. M., Gent, P. R., Ghan, S., Kay, J. E., Kushner, P. J., et al. (2013). The Community Earth System Model: A framework for collaborative research. *Bulleting of the American Meteorological Society*, *94*, 1339–1360.

Hurrell, J. W., Hack, J. J., Shea, D., Caron, J. M., & Rosinski, J. (2008). A new sea surface temperature and sea ice boundary dataset for the Community Atmosphere Model. *Journal of Climate*, *21*, 5145–5153. https://doi.org/10.1175/2008JCLI2292.1

Kalnay, E., Kanamitsu, M., Kistler, R., Collins, W., Deaven, D., Gandin, L., et al. (1996). The NCEP/NCAR 40-year reanalysis project. *Bulletin of the American Meteorological Society*, *77*, 437–471. https://doi.org/10.1175/1520-0477(1996)077<0437:TNYRP>2.0.CO;2

Landrum, L., Otto-Bliesner, B., Wahl, E. R., Conley, A., Lawrence, P., Rosenbloom, N., & Teng, H. (2013). Last millennium climate and its variability in CCSM4. *Journal of Climate*, *26*, 1085–1111. https://doi.org/10.1175/JCLI-D-11-00326.1

Lin, S. J., & Rood, R. B. (1997). An explicit flux-form semi-Lagrangian transport shallow water model on the sphere. *Quarterly Journal of the Royal Meteorological Society*, *123*, 2531–2533. https://doi.org/10.1002/qj.49712354416

Mann, M. E., Zhang, Z., Rutherford, S., Bradley, R. S., Hughes, M. K., Shindell, D., et al. (2009). Global signatures and dynamical origins of Little Ice Age and medieval climate anomalies. *Science*, *326*, 1256–1260. https://doi.org/10.1126/science.1177303

Newman, M., Alexander, M. A., Ault, T. R., Cobb, K. M., Deser, C., Di Lorenzo, E., et al. (2016). The Pacific Decadal Oscillation, revisited. *Journal of Climate*, *29*, 4399–4427. https://doi.org/10.1175/JCLI-D-15-0508.1

Osborn, T. J., & Jones, P. D. (2014). The CRUTEM4 land-surface air temperature data set: Construction, previous versions and dissemination via Google Earth. *Earth System Science Data*, *6*, 61–68. https://doi.org/10.5194/essd-6-61-2014

Otto-Bliesner, B., Brady, E. C., Fasullo, J., Jahn, A., Landrum, L., Stevenson, S., et al. (2016). Climate variability and change since 850 CE: An ensemble approach with the Community Earth System Model. *Bulletin of the American Meteorological Society*, *97*, 735–754. https://doi.org/10.1175/bams-d-14-00233.1

Palmer, W. C. (1965). *Meteorological drought* (pp. 1–58). Berkeley Springs, WV: U.S. Department of Commerce, Weather Bureau.

Phillips, T. J. (1996). Documentation of the AMIP models on the World Wide Web. *Bulletin of the American Meteorological Society*, *77*, 1191–1196. https://doi.org/10.1175/1520-0477(1996)077<1191:DOTAMO>2.0.CO;2

Rayner, N. A., Parker, D. E., Horton, E. B., Folland, C. K., Alexander, V., Rowell, D. P., et al. (2003). Global analyses of sea surface temperature, sea ice, and night marine air temperature since the late nineteenth century. *Journal of Geophysical Research*, *108*(D14), 4407. https://doi.org/10.1029/2002JD002670

Seager, R. Y., Kushnir, C., Herweijer, N. N., & Velez, J. (2005). Modeling of tropical forcing of persistent droughts and pluvials over western North America: 1856–2000. *Journal of Climate*, *18*(19), 4065–4088. https://doi.org/10.1175/JCLI3522.1

Sheffield, J., Wood, E. F., & Roderick, M. L. (2012). Little change in global drought over the past 60 years. *Nature*, *491*, 435–438. https://doi.org/10.1038/nature11575

Smith, T. M., Reynolds, R. W., Peterson, T. C., & Lawrimore, J. (2008). Improvements to NOAA's historical merged land–ocean surface temperature analysis (1880–2006). *Journal of Climate*, *21*, 2283–2296. https://doi.org/10.1175/2007JCLI2100.1

Smith, T. M., Reynolds, R. W., Peterson, T. C., & Lawrimore, J. (2010). Extended Reconstructed Sea Surface Temperature (ERSST) Monthly Analysis Version 3b. [Dataset]. NOAA National Climatic Data Center. https://doi.org/10.7289/V5Z31WJ4

Steiger, N. J., Smerdon, J. E., Cook, B. I., Seager, R., Williams, A. P., & Cook, E. R. (2019). Oceanic and radiative forcing of medieval megadroughts in the American Southwest. *Science Advances*, *5*(7), eaax0087. https://doi.org/10.1126/sciadv.aax0087

Steiger, N. J., Smerdon, J. E., Seager, R., Williams, A. P., & Varuolo-Clarke, A. M. (2021). ENSO-driven coupled megadroughts in North and South America over the last millennium. *Nature Geoscience*, *14*, 739–744. https://doi.org/10.1038/s41561-021-00819-9

Stevenson, S., Otto-Bliesner, B., Fasullo, J., & Brady, E. (2016). "El Niño like" hydroclimate responses to last millennium volcanic eruptions. *Journal of Climate*, *29*, 2907–2921. https://doi.org/10.1175/JCLI-D-15-0239.1

Stevenson, S., Overpeck, J. T., Fasullo, J., Coats, S., Parsons, L., Otto-Bliesner, B., et al. (2018). Climate variability, volcanic forcing, and last millennium hydroclimate extremes. *Journal of Climate*, *31*, 4309–4327. https://doi.org/10.1175/JCLI-D-17-0407.1

Stevenson, S., Timmermann, A., Chikamoto, Y., Langford, S., & DiNezio, P. (2015). Stochastically generated North American megadroughts. *Journal of Climate*, *28*, 1865–1880. https://doi.org/10.1175/JCLI-D-13-00689.1

Taylor, K. E., Williamson, D., & Zwiers, F. (2000). The sea surface temperature and sea-ice concentration boundary conditions for AMIP II simulations (PCMDI Report No. 60, 24).

Trenberth, K. E. (1997). The definition of El Niño. *Bulletin of the American Meteorological Society*, *78*(12), 2771–2777. https://doi.org/10.1175/1520-0477(1997)078<2771:TDOENO>2.0.CO;2

van der Schrier, G., Jones, P. D., & Briffa, K. R. (2011). The sensitivity of the PDSI to the Thornthwaite and Penman–Monteith parameterizations for potential evapotranspiration. *Journal of Geophysical Research*, *116*, D03106. https://doi.org/10.1029/2010JD015001

Webster, P. J., & Lukas, R. (1992). TOGA COARE: The coupled ocean–atmosphere response experiment. *Bulletin of the American Meteorological Society*, *73*, 1377–1416. https://doi.org/10.1175/1520-0477(1992)073<1377:TCTCOR>2.0.CO;2

Wilks, D. S. (1997). Resampling hypothesis tests or autocorrelated fields. *Journal of Climate*, *10*, 65–82. https://doi.org/10.1175/1520-0442(1997)010<0065:RHTFAF>2.0.CO;2

Wilks, D. S. (2011). *Statistical methods in the atmospheric sciences* (p. 676). London: Academic Press/Elsevier.

Woodhouse, C. A., & Overpeck, J. T. (1998). 2000 years of drought variability in the central United Stated. *Bulleting of the American Meteorological Society*, *79*, 2693–2714. https://doi.org/10.1175/1520-0477(1998)079<2693:YODVIT>2.0.CO;2